International Journal of Non-Linear Mechanics 57 (2013) 10–15

Contents lists available at SciVerse ScienceDirect

International Journal of Non-Linear Mechanics

journal homepage: www.elsevier.com/locate/nlm

Analysis of laser power threshold for self oscillation in thermo-optically excited doubly supported MEMS beams

David Blocher*, Richard H. Rand, Alan T. Zehnder

Field of Theoretical and Applied Mechanics, Cornell University, Ithaca, NY 14853, USA

ARTICLE INFO

Article history:
Received 18 December 2011
Received in revised form
12 June 2013
Accepted 13 June 2013
Available online 21 June 2013

Keywords:
MEMS
Limit cycle
Hopf bifurcation
Numerical continuation
Resonator

ABSTRACT

An optically thin MEMS beam suspended above a substrate and illuminated with a CW laser forms an interferometer, coupling out-of-plane deflection of the beam to absorption within it. In turn, laser absorption creates thermal stresses which drive further deflection. This coupling of motion to thermal stresses can cause limit cycle oscillations in which the beam vibrates in the absence of periodic external forcing. Prior work has modeled such thermal–mechanical systems using ad-hoc coupled ordinary differential equations, with finite element analysis (FEA) used to fit model parameters. In this paper we derive a first principles model of such oscillations from the continuum description of the temperature and displacement field. A bifurcation analysis of the model is performed, allowing us to easily estimate the threshold power for self-oscillation as a function of geometric and optical constants of the beam.

© 2013 Elsevier Ltd. All rights reserved.

1. Introduction

Due to their high frequency, microelectromechanical system (MEMS) resonators have been proposed for a number of different sensing [1] and signal processing [2–4] applications in the past decade. Typically, MEMs resonators are capacitively or piezoelectrically driven using a sinusoidal signal. Shifts in their resonant frequency or phase relationship can be used to infer a measurement or perform a calculation. Such drive methods require an external, highly stable frequency source and additional conductive or piezoelectric material layers on the device. Optical excitation methods can produce self-oscillation without the need for an external periodic excitation, or additional device layers.

Previous work [5–7] has shown that an optically thin MEMS device suspended over a substrate sets up a Fabry–Pérot interferometer which couples absorption and deflection. Illuminating the device with a continuous wave (CW) unmodulated laser causes optical–thermal–mechanical feedback. For low laser power, the device will bend statically, but for high enough laser power it has been observed experimentally [8] that such devices may undergo a Hopf-bifurcation leading to self-oscillation. Similar phenomena include thermal–mechanical feedback oscillations in satellites subjected to solar radiation [9], and aero-elastic feedback oscillations (flutter) in aircraft [10].

For interferometric transduction of MEMS resonators to be a viable means of producing periodic motion, first its causes must be understood, and then models developed that predict the minimum laser power needed for self-oscillation. Several researchers have given explanations of the causes of self-oscillation. Churenkov [6] examined beams with surface coatings and showed that differing coefficients of thermal expansion between the beam material and surface coating could cause bending moments that drive oscillation. Langdon and Dowe [5] assumed that energy was absorbed near the top surface and that vertical thermal gradients caused bending moments which drove self-oscillation. Both use energy methods to derive formulae for the minimum laser power needed to sustain oscillation. However, we have shown [11] that the mechanical–thermal coupling in uncoated pre-buckled beams is due to asymmetry of the anchor support, and not the bi-metallic effect or vertical thermal gradients. Sekaric et al. gives a semi-empirical formula for the threshold power for self-oscillation in [12] based on measured frequency shifts due to heating, though no model of the dynamics. Gigan et al. have suggested that radiation pressure may drive self-oscillation in beams coated for high reflectivity [13–15]. In this work we consider only photo-thermal forces.

Models of device dynamics have also been constructed. Variations of a coupled oscillator model are used to model device dynamics in [8,16–19]. Perturbation theory is used to estimate the threshold power for self-oscillation in [8,16]. Such models provide accurate predictions of the transition power to self-oscillation for specific devices, but would require parametric FEA to study, e.g. the impact of device geometry on the transition power.

* Corresponding author. Tel.: +1 607 255 0824; fax: +1 607 255 2011.
E-mail address: dbb74@cornell.edu (D. Blocher).

0020-7462/$ - see front matter © 2013 Elsevier Ltd. All rights reserved.
http://dx.doi.org/10.1016/j.ijnonlinmec.2013.06.010

Motivated by the need to understand the contributors to low power self-resonant devices at the level of device design, in this paper we sacrifice accuracy for ease of use and present an (almost) parameter free model of interferometrically driven self-resonant MEMS. Initially straight, doubly supported beams are chosen due to their simple geometry and wide-spread application. Perturbation analysis is used to predict the threshold power for self-oscillation, and predictions compared with the results of numerical continuation. Scalings of threshold power with device geometry and pre-stress are discussed.

2. Mathematical model

Our analysis models doubly supported MEMS beams illuminated with a CW laser focused to a spot at their center. A beam theory model which incorporates in-plane tension is used to model the displacement field of the beam. Device imperfections are an important source of thermal–mechanical coupling in doubly supported beams [11] and are incorporated later in the model. The temperature field is also modeled as a one-dimensional continuum governed by a first order thermal equation. Finally, an optical model determines the laser power absorbed as a function of the beam's center displacement. These two partial differential equations (PDEs) and one algebraic equation describe the optical-thermal–mechanical feedback in the device. A Galerkin projection is used to approximate the PDEs as a set of coupled ordinary differential equations (ODEs), and an imperfection term is added to account for asymmetry of the support. Finally bifurcation analysis of the ODEs is used to estimate the threshold laser power for self-oscillation.

To begin with, we use beam theory to model the mechanical behavior of the beam. Our model is adapted from an equation for the vibration of a beam including membrane stiffness. Only the details are sketched here, and the reader is referred to the original paper [20] for further details. Letting x be the position along the beam, $y(x)$ be the lateral deflection at point x, and including the effects of membrane stress

$$M[y,U] = EIy'''' + Fy'' + m\ddot{y} + \zeta\dot{y} = 0, \tag{1}$$

where m is the mass per unit length, ζ is the viscous damping coefficient, EI is the flexural rigidity, F is the force of tension in the beam, primes denote spatial derivatives, and overdots denote time derivatives. In plane forces arise from residual tension, thermal expansion, and deflection. Using linear thermo-elasticity and writing the axial extension due to deflection to first order, the force of tension, F, is

$$F = \sigma A - \frac{EA}{L}\int_0^L \alpha_e U(x)dx + \frac{EA}{2L}\int_0^L (y'(x))^2 dx, \tag{2}$$

where σ is the residual tensile stress, A is the cross-sectional area of the beam, L is the length, α_e is the coefficient of thermal expansion, and $U(x)$ is the temperature above ambient. The sign convention is that positive loads are tensile and negative loads are compressive. The beam is clamped on both ends giving the boundary conditions

$$y(0) = y(L) = 0, \quad y'(0) = y'(L) = 0. \tag{3}$$

Fourier's law is used to model the temperature field. Since MEMS resonators are often used in low pressure environments to reduce damping, convective heat loss can be ignored. Furthermore, radiative heat loss is negligible for the modest temperature rises predicted. Finally, it has been shown that through thickness thermal gradients are negligible [11]. Thus we model the temperature in the beam using a simple 1D thermal model. Letting $\dot{q}(x)$ be the heat generated per unit volume, and assuming that the temperature above ambient is zero at the ends, we get

$$H[y,U] = \dot{U} - \alpha_c U'' - \frac{1}{\rho c}\dot{q}(x) = 0; \quad U(0) = U(L) = 0. \tag{4}$$

where α_c is the thermal diffusivity, ρ is the mass density, and c is the specific heat capacity. Note that our thermal boundary conditions (4) assume that the substrate acts as an infinite heat sink.

The heating $\dot{q}(x)$ depends on the total laser power P, spatial power distribution, and on the fraction, $f(x)$, of power absorbed at a given distance along the beam. Due to the Fabry–Pérot interferometer between the beam and substrate, $f(x)$ depends on x through the displacement field $y(x)$. Using the optical properties of the films involved, and their thicknesses, $f(y(x))$ can be solved for numerically [21]. However the bifurcation to limit cycle oscillations depends on this function only in the neighborhood of the fixed point, and so we use a Taylor series approximation about zero-deflection.[1] Assuming that the laser power is focused to a spot at the beam's centerline we get

$$\dot{q}(x) = \frac{P}{A}[\alpha_o + \gamma y(x)]\delta\left(x - \frac{L}{2}\right), \tag{5}$$

where P is the total laser power, α_o is the zero-deflection absorption, γ is the contrast of the Fabry–Pérot interferometer, and the delta-function, δ, is our spatial power distribution.

Finally, our equations are projected onto a set of test functions using the Galerkin method, and a set of coupled, non-linear ODEs obtained. For our test functions we select a time-dependent weight function multiplied by a space dependent shape function

$$\tilde{y}(x,t) = a(t)\left(1 - \cos\left(\frac{2\pi x}{L}\right)\right), \quad \tilde{U}(x,t) = b(t)\sin\left(\frac{\pi x}{L}\right). \tag{6}$$

Note that our test functions satisfy the boundary conditions (3) and (4) regardless of the time dependent weight functions. Requiring that our error in approximation be orthogonal to the test functions gives 2 ODEs governing the weight functions

$$\int_0^L \tilde{y}(x,t) M[\tilde{y}(x,t), \tilde{U}(x,t)]dx = 0 \rightarrow \ddot{a} + c_0\dot{a} + c_1 a + c_2 a^3 = c_3 ab, \tag{7}$$

$$\int_0^L \tilde{U}(x,t) H[\tilde{y}(x,t), \tilde{U}(x,t)]dx = 0 \rightarrow \dot{b} = -c_4 b + \frac{2P}{mcL}[\alpha_o + 2\gamma a], \tag{8}$$

with the constants c_i defined as follows:

$$c_0 = \frac{\zeta}{m}$$

$$c_1 = \left[\frac{4\pi^2\sigma A}{3\,mL^2} + \frac{16\pi^4 EI}{3\,mL^4}\right]$$

$$c_2 = \left[\frac{4\pi^4 AE}{3\,mL^4}\right]$$

$$c_3 = \left[\frac{8\pi\alpha_e AE}{3\,mL^2}\right]$$

$$c_4 = \left[\frac{\pi^2\alpha_c}{L^2}\right].$$

Our thermal Eq. (8) is a simple first order thermal equation coupled to the mechanical Eq. (7) through the $2P/mcL[\alpha_o + 2\gamma a]$ term. The mechanical equation is in the form of a damped Duffing oscillator coupled to the thermal equation through the c_{3ab} term. If we neglect the damping and non-linear terms in (7) then our linearized mechanical equation demonstrates the correct frequency relationship inherent in Euler buckling and correctly

[1] This approximation eliminates the periodicity of the interference field and suppresses some phenomenon in the post-Hopf dynamics such as spectral distortion [7,22], limiting amplitude [23], and multi-mode oscillations [23,22]. To first order, it has no impacted on the predicted value of P_{Hopf}.

predicts the buckling load [24]. For a fixed level of pre-stress, thermal buckling is also possible in the model due to laser heating.

Note that $(a_{eq}=0,\ b_{eq}=2P\alpha_o/mcc_4L)$ is always an equilibrium solution to Eqs. (7) and (8) which thus exhibit perfect buckling. As has been noted in [11], this means that until buckling is reached a_{eq} will be independent of P, i.e. displacement will be independent of heating. However, in the physical system, asymmetry of the support, initial shape imperfections, or fabrication defects break the symmetry and lead to imperfection buckling where there is a small non-zero deflection before the buckling load. The most common technique for dealing with these asymmetries analytically is to lump all contributors to asymmetry together into a net imperfection modeled as small amplitude pre-deformation of the beam in it's first buckling mode. The beam's amplitude of imperfection is typically unknown in advance, and would become a fitting parameter in the system [25]. As such, rather than incorporating the effect of imperfections at the stage of PDEs, we choose to do so at the stage of ODEs, by adding a direct thermal–mechanical coupling term, c_{5b}, to the mechanical equation which breaks the symmetry and gives a_{eq} a non-zero value pre-buckling. This term can be directly related to the measurable change in deflection per unit temperature rise [11].

Including this imperfection term, and re-writing (7) and (8) in first order form with the change of variables $a\to z$; $\dot{a}\to v$; $b\to T$ we get our model equations:

$$\begin{bmatrix}\dot{z}\\ \dot{v}\\ \dot{T}\end{bmatrix}=\begin{bmatrix}v\\ -c_0v-c_1z-c_2z^3+c_3zT+c_5T\\ -c_4T+\frac{2P}{mcL}(\alpha_o+2\gamma z)\end{bmatrix}, \tag{9}$$

where T is the centerline beam temperature above ambient, z is the centerline beam displacement, and v is the velocity of the centerline.

3. Bifurcation analysis

Since the transition to self-oscillation has been shown to happen in a Hopf bifurcation [8], we analyze our Eqs. (9) for the laser power, P_{Hopf}, which causes this bifurcation. We calculate the steady state deflection and temperature as a function of laser power, P, linearize the system about this equilibrium solution, and then check for a pair of pure imaginary eigenvalues in the linearized system.

Plugging in the equilibrium condition $\dot{z}=\dot{v}=\dot{T}=0$ we get an algebraic equation for the location $[z_{eq},v_{eq},T_{eq}]$ of the equilibrium point. One equation is trivially $v_{eq}=0$. While unwieldy closed form solutions exist for the other two, we sacrifice accuracy for manageability by estimating the equilibrium solution using a perturbation series.

In the pre-buckling regime, the deflection is dominated by the imperfection level. We let $P=\epsilon P,\ z_{eq}=z_0+\epsilon z_1+\epsilon^2 z_2+\cdots$ and collect powers in ϵ to get to lowest order

$$z_{eq}^{pre}(P)=\frac{2\alpha_o c_5}{c_1c_4mcL}P$$
$$T_{eq}^{pre}(P)=\frac{2P}{c_4mcL}\left[\alpha_o+2\gamma z_{eq}^{pre}\right], \tag{10}$$

In the post-buckling regime, deflection is governed by the linear and non-linear stiffness, and the imperfection level is irrelevant. We let $c_5=\epsilon c_5,\ z_{eq}=z_0+\epsilon z_1+\epsilon^2 z_2+\cdots$ to get

$$z_{eq}^{post}(P)=\frac{\sqrt{4c_3^2P^2\gamma^2-c_1c_2c^2\,m^2L^2c_4^2+2\alpha_oc_2c_3c_4mcLP}+2c_3\gamma P}{c_2c_4mcL}$$
$$T_{eq}^{post}(P)=\frac{2P}{c_4mcL}\left[\alpha_o+2\gamma z_{eq}^{post}\right], \tag{11}$$

Evaluating the Jacobian at the estimated equilibrium point, we get the following characteristic equation for the eigenvalues:

$$\lambda^3+k_2\lambda^2+k_1\lambda+k_0=0, \tag{12}$$

where k_i depend on P through $z_{eq}(P)$ and $T_{eq}(P)$. Letting $\lambda=\pm i\omega$ and equating the real and imaginary parts yields the following equation on P_{Hopf}:

$$k_0(P_{Hopf})=k_1(P_{Hopf})\cdot k_2(P_{Hopf});\ \ k_0(P_{Hopf})>0. \tag{13}$$

In the pre-buckled regime we use (10) for the equilibrium solution $[z_{eq}(P),0,T_{eq}(P)]$. This gives a quadratic on P_{Hopf} in terms of the model parameters. In order to determine which root is extraneous, we note that as $c_5\to 0$, heating and displacement are uncoupled in this regime and $P_{Hopf}\to\infty$. Thus we keep the root which comes in from infinity, and is positive

$$k_0^{pre}(P)=-\frac{4c_5\gamma P}{mcL}-\frac{16\alpha_oc_3c_5\gamma P^2}{c_1c_4m^2c^2L^2}-\frac{2\alpha_oc_3P}{mcL}+\frac{12c_2\alpha_o^2c_5^2P^2}{c_4c_1^2\,m^2c^2L^2}+c_1c_4 \tag{14}$$

$$k_1^{pre}(P)=-\frac{8\alpha_oc_3c_5\gamma P^2}{c_1c_4^2\,m^2c^2L^2}-\frac{2\alpha_oc_3P}{c_4mcL}+\frac{12c_2c_5^2\alpha_o^2P^2}{c_1^2c_4^2\,m^2c^2L^2}+c_0c_4+c_1 \tag{15}$$

$$k_2^{pre}(P)=c_4+c_0 \tag{16}$$

In the post-buckled regime we use (11) for the equilibrium solution and get an implicit equation for P_{Hopf}:

$$\begin{aligned}k_0^{post}(P)=&\frac{4c_3\gamma P\sqrt{4c_3^2\gamma^2P^2-c_1c_2c_4^2\,m^2c^2L^2+2\alpha_oc_2c_3c_4mcLP}}{c_2c_4mcL^2}\\&+\frac{8c_3^2\gamma^2P^2}{c_2c_4m^2c^2L^2}+4P\frac{\alpha_oc_3-c_5\gamma}{mcL}-2c_1c_4\\k_1^{post}(P)=&\frac{8c_3\gamma P\sqrt{4c_3^2\gamma^2P^2-c_1c_2c_4^2\,m^2c^2L^2+2\alpha_oc_2c_3c_4mcLP}}{c_2c_4^2\,m^2c^2L^2}\\&+\frac{16c_3^2\gamma^2P^2}{c_2c_4^2\,m^2c^2L^2}+\frac{4\alpha_oc_3P}{c_4mcL}+c_0c_4-2c_1k_2^{post}(P)=c_4+c_0\end{aligned} \tag{17}$$

Eqs. (13–15) form an implicit equation for P_{Hopf}. In (5) these formula will be numerically evaluated using a root-finding method and the results compared with continuation results for physically relevant parameters.

4. Parameter fitting

While our first-principals derivation of the governing equations skirts the need for time consuming FEA to fit model parameters, there are still two parameters which require analysis: the damping constant, c_0, and the thermal–mechanical coupling constant, c_5. In this section we present those analyses and give the values for the material and geometric properties used in calculating the other parameters.

There are many sources of damping in MEMS, including viscous or squeeze-film damping, thermo-elastic damping, and clamping losses [26]. Rather than relating the damping term c_0 to these environment factors, we relate it to the measurable quality factor Q of the mechanical resonator. Driven at low laser power, the intrinsic quality factor Q can be measured. In this situation, our Eqs. (9) reduce to $\ddot{z}+c_0\dot{z}+c_1z+c_2z^3=0$. In the pre-buckled regime $(c_1>0)$ the only equilibrium is $z_{eq}=0$ and linearized frequency is simply $\sqrt{c_1}$. We get damping term $c_0=\sqrt{c_1}/Q$ by comparison of the linearized equation to the simple harmonic oscillator, $\ddot{z}+\omega_o/Q(\dot{z})+\omega_0^2z=0$. In the post-buckled regime $(c_1<0)$, we have $z_{eq}=\sqrt{-c_1/c_2}$ and linearized frequency of $\sqrt{-2c_1}$ giving $c_0=\sqrt{-2c_1}/Q$. Note that our calculation of the pre- and post-buckled frequency agrees quite well with those given in [27].

As previously mentioned, our thermal–mechanical coupling constant, c_5, can be related to the change in displacement per unit temperature rise. Doing a perturbation series approximation in T to our mechanical equation about the $z=0$ equilibrium we get the following relationship for the equilibrium solution $z_{eq} = \frac{c_5}{\gamma} c_1(T_{eq}) + \mathcal{O}(T^2)$. To fit c_5 one could heat the sample, measure the displacement and take the ratio, scaled by c_1. FEM data on the imperfection level of a 15 μm beam is presented in [11], and experimental data for beams of length 30–140 μm in [25]. The imperfection amplitude is assumed to scale as the length of the beam [25], thus $c_5/c_1 L$ is a constant. Using the data in [11] we get a change in displacement per unit temperature rise per unit length of $c_5/c_1 L = 5 \times 10^{-7} 1/K$, in close agreement with $c_5/c_1 L = 1 \times 10^{-6} 1/K$ from [25].

Material and geometric parameters used in subsequent numerical results are given below. Optical parameters (α_o, γ) are fit using a physics based model of reflection, transmission and absorption in thin films given in [21]. Note that the equilibrium value shifts with pre-stress or heating, particular for buckled beams. For buckled beams, if the buckling amplitude is a significant fraction of the period of the interference field, one would need to include the buckling amplitude when calculating the absorption function. The shift in equilibrium due to heating, or pre-stress in the non-buckled regime is negligible.

Parameter	Value
E	130 (GPa)
m	1.22×10^{-9} (kg/m)
α_e	2.5×10^{-6} $(1/K)$
α_o	0.043
Q	10,000
c	712 (J/kgK)
σ	Continuation parameter (Pa)
I	1.69×10^{-27} (m^4)
A	5.03×10^{-13} (m^2)
α_c	9.87×10^{-5} (m^2/s)
γ	-9×10^4 $(1/m)$
$c_5/c_1 L$	5×10^{-7} $(1/K)$
L	Continuation parameter (m)
P	Continuation parameter (W)

5. Numerical results

The continuation tool AUTO 2000 [28] is used to examine the nature of solutions to (9). This software package is commonly used in bifurcation analysis of differential equations and algebraic systems. Using AUTO, we can calculate P_{Hopf} as a function of the beam's length and pre-stress level in order to verify the analytic estimate of $P_{Hopf}(L, \sigma)$ found using perturbation theory.

We treat L, σ, and P as our continuation parameters, and start with $L = 10$ μm, $\sigma = 0$, $P=0$ which has known equilibrium value $[x_{eq} = 0, v_{eq} = 0, T_{eq} = 0]$. We then continue this equilibrium solution in P, monitoring the eigenvalues of the Jacobian of the linearized system for Hopf bifurcations. Once we reach $P_{Hopf}(10, 0)$, we switch parameters, and continuing the Hopf point in L and σ. In this way we can trace out the surface $P_{Hopf}(L, \sigma)$. Due to the singular nature of the buckling point, we cannot continue solutions across it. In order to trace out the post-buckled surface, we calculate an equilibrium solution in the buckled regime $(\sigma = 2\sigma_B)$ using a root-finding routine, and repeat the process of finding $P_{Hopf}(10, 2\sigma_B)$ and continuing it in L and σ in that region. The stress required to produce buckling depends on beam length. In order to compare results for beams of different lengths, we scale the residual stress by the buckling stress, plotting the buckling parameter $\overline{p} = \sigma/\sigma_B$ as our non-dimensional measure of stress (see Fig. 1).

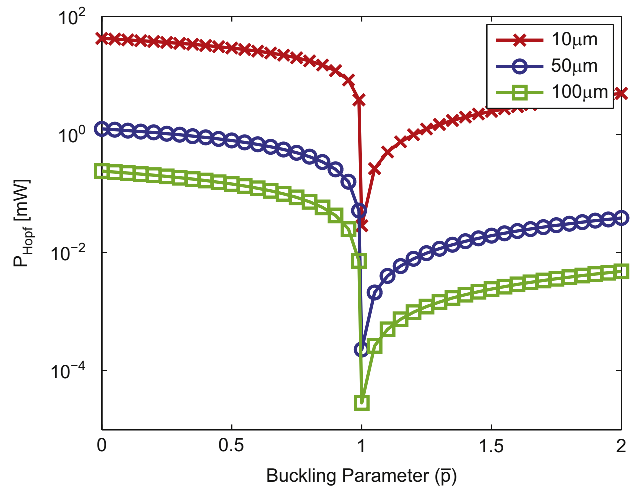

Fig. 1. Threshold power for self-oscillation, P_{Hopf}, calculated using continuation theory, and plotted as a function of buckling parameter $\overline{p}$ for fixed length. Note that $\overline{p} = 1$ is the buckling load.

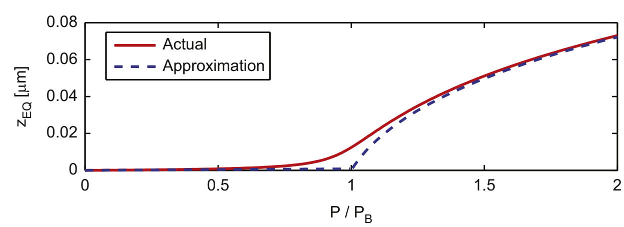

Fig. 2. AUTO calculated and approximate equilibrium solutions as a function of laser power P. Data is for a 50 μm beam with no initial pre-stress. Note that our approximations (10, 11) lose accuracy near the thermal buckling load where the slope of the load curve is most nearly vertical.

Note that P_{Hopf} decreases with length for a fixed buckling parameter. For fixed length, P_{Hopf} is lowest at buckling, where it appears to go to zero. We believe this is because of the strength of coupling between heating and displacement in this region. As the level of pre-stress approaches the buckling load, the slope of the load curve becomes almost vertical at the (imperfect) buckling point (see Fig. 2). As a result, heating is most strongly coupled to displacement near buckling, giving strong feedback. In the post buckled region, the slope of the load curve tapers off, leading to a decrease in coupling and increase in P_{Hopf}.

We find the main drivers of self-oscillation to be the strength of coupling of absorption to displacement and of thermal stress to displacement. The former is described by the absorption contrast, requiring accurate knowledge of film thickness and optical properties. As mentioned previously, the latter is dominated by stress level in the post-buckled beams, and imperfection level in the pre-buckled beams. While stress in thin-films is relatively easy to predict and characterize, imperfection levels are generally unknown in advance, making predictions of P_{Hopf} more challenging for pre-buckled beams.

In order to verify our perturbation results, we compare the estimates of (14, 15) to the results of numerical continuation (see Fig. 3). Note that our approximations of P_{Hopf} lose accuracy near the buckling load and are worse in the pre-buckled regime where our equilibrium value approximations are worse. Higher order approximations of the equilibrium point give more accurate

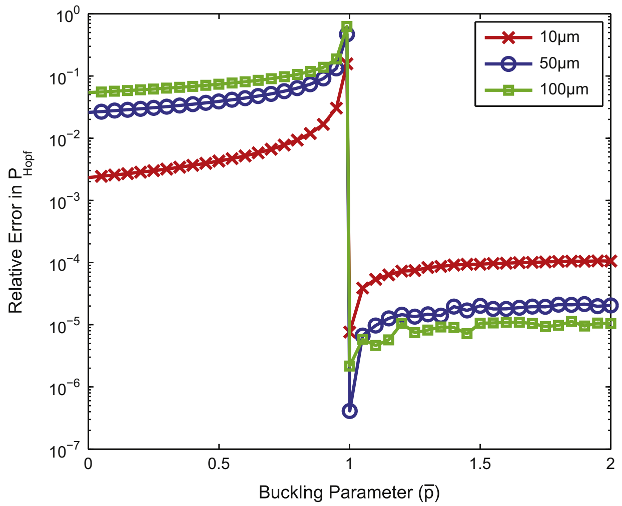

Fig. 3. Relative error in perturbation approximation of P_{Hopf} as compared with actual result found using numerical continuation.

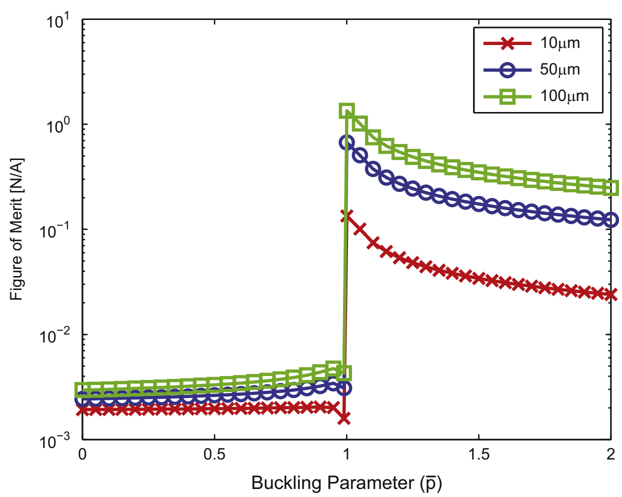

Fig. 4. Relative figure of merit for self-resonant MEMS. Results are scaled to unity maximum.

results, but yield unwieldy formulas for P_{Hopf}. While the threshold power for self-oscillation is predicted to decrease drastically near buckling, the frequency also goes to zero. In practical applications, low threshold powers of self-oscillation and high frequencies are both desirable. Thus, a good figure of merit for a self-resonant beam would be

$$\text{F.O.M.} = \frac{\text{resonant frequency}}{\text{threshold power for self}-\text{oscillation}}$$

In Fig. 4 we plot the figure of merit for the beams under consideration. Longer, just barely buckled beams have the highest figure of merit.

6. Conclusion

A MEMS device, illuminated within an interference field may self-oscillate due to feedback between heating and absorption. Prior work on modeling the dynamics of such devices has used ad-hoc models and fit model parameters using an number of extensive FEA calculations. In this paper we use a first-principles method to derive the model equations without need for extensive parameter estimation analyses. Quantitative accuracy is sacrificed for the sake of implicit equations for the threshold power for self-oscillation from which conclusions can be drawn about the qualitative device features leading to low power self-oscillation. Predicted values of P_{Hopf} are compared with the results of numerical continuation, and a parametric study is performed, varying device length and level of pre-stress. Results support the prediction in [11] that barely post-buckled beams should have the lowest threshold power for self-oscillation. More specifically, results show that the value of P_{Hopf} is dominated by the slope of the load curve. In the post-buckled region, this slope is determined by the buckling parameter, whereas in the pre-buckled region, it is determined by the level of imperfection—a parameter which is difficult to control experimentally.

Acknowledgment

This work was partially supported under the CMS NSF grant CMS-0600174 “Nonlinear Dynamics of Coupled MEMS Oscillators.”

References

[1] B.R. Ilic, D.A. Czaplewski, H.G. Craighead, P. Neuzil, C. Campagnolo, C.A. Batt, Mechanical resonant immunospecific biological detector, Applied Physics Letters 77 (2000) 450–452, http://dx.doi.org/10.1063/1.127006.
[2] A. Uranga, J. Verd, J. López, J. Teva, G. Abadal, F. Torres, J. Esteve, F. Pérez Murano, N. Barniol, Fully integrated MIXLER based VHF CMOS-MEMS clamped-clamped beam resonator, Electronics Letters 48 (8) (2007) 452–454, http://dx.doi.org/10.1049/el:20070580.
[3] L. Lin, R.T. Howe, A.P. Pisano, Microelectromechanical filters for signal processing, Journal of Microelectromechanical Systems 7 (3) (1998) 286–294, http://dx.doi.org/10.1109/84.709645.
[4] F.C. Hoppensteadt, E.M. Izhikevich, Synchronization of MEMS resonators and mechanical neurocomputing, IEEE Transactions on Circuits and Systems—I: Fundamental Theory and Applications 48 (2) (2001) 133–138, http://dx.doi.org/10.1109/81.904877.
[5] R. Langdon, D. Dowe, Photoacoustic oscillator sensors, in: SPIE Conf. Fiber Opt. Sens., 1987, pp. 86–93.
[6] A. Churenkov, Photothermal excitation and self-excitation of silicon micro-resonators, Sensors and Actuators A 39 (1993) 141–148, http://dx.doi.org/10.1016/0924-4247(93)80211-X.
[7] N. Stokes, R.M. Fatah, S. Venkatesh, Self-excitation in fiber-optic microresonator sensors, Sensors and Actuators A 21 (1990) 369–372, http://dx.doi.org/10.1016/0924-4247(90)85073-D.
[8] K.L. Aubin, M.K. Zalalutdinov, T. Alan, R.B. Reichenbach, R.H. Rand, A.T. Zehnder, J.M. Parpia, H.G. Craighead, Limit cycle oscillations in CW laser-driven NEMS, Journal of Microelectromechanical Systems 13 (6) (2004) 1018–1026 http://dx.doi.org/10.1.1.151.6977.
[9] E.A. Thornton, Thermal Structures for Aerospace Applications, American Institute of Aeronautics and Astronautics (1996).
[10] E.H. Dowell, E.F. Crawley, H.C. Curtiss Jr., D.A. Peters, R.H. Scanlan, F. Sisto (Eds.), A Modern Course in Aeroelasticity Solid Mechanics and its Applications, 3rd edition, Springer, 1995.
[11] D.B. Blocher, A.T. Zehnder, R.H. Rand , S. Mukerji, Anchor deformations drive limit cycle oscillations in interferometrically transduced MEMS beams, Finite Elements in Analysis and Design 49 (1) (2012) 52–57. http://dx.doi.org/10.1016/j.finel.2011.08.020.
[12] L. Sekaric, M.K. Zalalutdinov, S.W. Turner, A.T. Zehnder, J.M. Parpia, H.G. Craighead, Nanomechanical resonant structures as tunable passive modulators of light, Applied Physics Letters 80 (19) (2002) 3617–3619, http://dx.doi.org/10.1063/1.1479209.
[13] O. Arcizet, P. Cohadon, T. Briant, M. Pinard, A. Heidmann, Radiation pressure cooling and optomechanical instability of a micromirror, Nature 444 (2006) 71–74, http://dx.doi.org/10.1038/nature05244.
[14] M.W. Pruessner, T.H. Stievater, J.B. Khurgin, W.S. Rabinovich, An integrated waveguide-DBR microcavity opto-mechanical system, Optics Express 19 (22) (2011) 21904–21918, http://dx.doi.org/10.1364/OE.19.021904.
[15] S. Gigan, H. Bohm, M. Paternostro, F. Blaser, G. Langer, J. Hertzberg, K. Schwab, D. Bauerle, M. Aspelmeyer, A. Zeilinger, Self-cooling of a micromirror by radiation pressure, Nature 444 (2006) 67–70, http://dx.doi.org/10.1038/nature05273.
[16] M.K. Zalalutdinov, J.M. Parpia, K.L. Aubin, H.G. Craighead, T. Alan, A.T. Zehnder, R.H. Rand, Hopf bifurcation in a disk-shaped NEMS, in: Proceedings of the 2003 ASME Design Engineering Technical Conferences, 19th Biennial Conference on Mechanical Vibrations and Noise, Chicago, IL, 2003, pp. 1759–1769.
[17] M.K. Zalalutdinov, A.T. Zehnder, A. Olkhovets, S.W. Turner, L. Sekaric, B.R. Ilic, D.A. Czaplewski, J.M. Parpia, H.G. Craighead, Autoparametric optical drive for

micromechanical oscillators, Applied Physics Letters 79 (5) (2001) 695–697, http://dx.doi.org/10.1063/1.1388869.
[18] M. Pandey, K.L. Aubin, M.K. Zalalutdinov, R.B. Reichenbach, A.T. Zehnder, R.H. Rand, H.G. Craighead, Analysis of frequency locking in optically driven MEMS resonators, Journal of Microelectromechanical Systems 15 (6) (2006) 1546–1554, http://dx.doi.org/10.1109/JMEMS.2006.879693.
[19] T. Sahai, R.B. Bhiladvala, A.T. Zehnder, Thermomechanical transitions in doubly-clamped micro-oscillators, International Journal of Non-Linear Mechanics 42 (4) (2007) 596–607, http://dx.doi.org/10.1016/j.ijnonlinmec.2006.12.009.
[20] J.G. Eisley, Nonlinear vibration of beams and rectangular plates, Journal of Applied Mathematics and Physics 15 (1964) 167–175, http://dx.doi.org/10.1007/BF01602658.
[21] L. Sekaric, Studies in NEMS: nanoscale dynamics, energy dissipation, and structural materials, Ph.D. Thesis, Cornell University, 2003.
[22] J. Li, S. Evoy, Study of laser-induced self-oscillations in silicon nanomechanical resonators, Journal of Applied Physics 98 (2005) 084316, http://dx.doi.org/10.1063/1.2099513.
[23] K. Hane, K. Suzuki, Self-excited vibration of a self-supporting thin film caused by laser irradiation, Sensors and Actuators A 51 (1996) 179–182, http://dx.doi.org/10.1016/0924-4247(95)01218-4.
[24] S.P. Timoshenko, Vibration Problems in Engineering, (3rd edition), D. Van Nostrand Company, Inc, 1955.
[25] W. Fang, J. Wickert, Post buckling of micromachined beams, Journal of Micromechanics and Microengineering 4 (1994) 116–122, http://dx.doi.org/10.1088/0960-1317/4/3/004.
[26] K.Y. Yasumura, T.D. Stowe, E.M. Chow, T. Pfafman, T.W. Kenny, B.C. Stipe, D. Rugar, Quality factors in micron- and submicron-thick cantilevers, Journal of Microelectromechanical Systems 9 (1) (2000) 117–125, http://dx.doi.org/10.1109/84.825786.
[27] S. Bouwstra, B. Geijselaers, On the resonance frequency of microbridges, in: Digest of Technical Papers, Solid-State Sensors & Actuators (Transducers'91), 1991, pp. 538–542. http://dx.doi.org/10.1109/SENSOR.1991.148932.
[28] E.J. Doedel, Lecture notes on numerical analysis of nonlinear equations, in: B. Krauskopf, H.M. Osinga, J. Gálan-Vioque (Eds.), Numerical Continuation Methods for Dynamical Systems: Path Following and Boundary Value Problems, Springer, 2007, pp. 1–49.